PHYSICAL REVIEW B **71**, 020102(R) (2005)

Diffuse x-ray scattering in perovskite ferroelectrics

B. D. Chapman,[1,*] E. A. Stern,[1,2,†] S.-W. Han,[1,‡] J. O. Cross,[2] G. T. Seidler,[1,2] V. Gavrilyatchenko,[3] R. V. Vedrinskii,[3] and V. L. Kraizman[3]

[1]*Department of Physics, University of Washington, Seattle, Washington 98195-1560, USA*

[2]*PNC-CAT, Sector 20, Advanced Photon Source, Argonne, Illinois 60439, USA*

[3]*Department of Physics, Rostov State University, Rostov, 344090 Russia*

(Received 11 November 2004; published 24 January 2005)

Diffuse x-ray scattering measurements on the cubic paraelectric phase of single-crystal $PbTiO_3$ are presented. No diffuse scattering sheets are found, in contrast to sheets observed in the cubic paraelectric phases of $BaTiO_3$ and $KNbO_3$. A quantitative analysis of the diffuse scattering indicates that the soft-mode branch contribution to sheets is negligible in all three ferroelectric perovskites. Differences in the diffuse scattering are explained by differences in the disordering of the local displacements, thus resolving a long-standing controversy.

DOI: 10.1103/PhysRevB.71.020102 PACS number(s): 77.80.Bh, 61.10.Eq, 64.70.Kb, 77.84.Dy

Understanding structural phase transitions is one of the central issues of condensed-matter physics. The nature of structural phase transitions in perovskite ferroelectrics has been intensely investigated because of their simple structure together with the importance of ferroelectricity as an interesting phenomenon with practical applications. Despite extensive studies of the perovskites, one fundamental issue of debate persists, namely, the origin of the reciprocal lattice space diffuse x-ray scattering (DXS) sheets in the paraelectric cubic phases of $BaTiO_3$ and $KNbO_3$.[1,2] Based on ideas from the pure displacive model introduced by Cochran,[3] the diffuse sheets were explained by Huller as the formation of linear chains of correlated displacements in the transverse optical (TO) soft mode.[4] The displacive model was based on the assumption that the soft mode becomes unstable as its frequency goes to zero on cooling to the tetragonal ferroelectric phase from the cubic paraelectric phase at the transition temperature T_C, and the lattice stabilizes with an off-cubic-site displacement to form the ferroelectric state. In the alternative Comes model of order-disorder,[1,5] the diffuse sheets are explained by the formation of linear chains of short-range correlated local displacements that exist in the paraelectric phase and have long-range order in the ferroelectric phase. The consensus soon after the experimental discovery of the DXS sheets was the soft-mode explanation because only it could explain the large Curie-Weiss factor in ferroelectricity.

However, subsequent experimental evidence indicated the soft mode never went to zero but became overdamped instead (the central peak). Later x-ray absorption fine-structure (XAFS) measurements of the local structure of $PbTiO_3$,[6] $BaTiO_3$ (Ref. 7), and $KNbO_3$ (Ref. 8) showed unambiguously the existence of local ferroelectric distortions in the cubic phases of these materials well above T_C. This finding was supported by additional, less definitive, experimental evidence,[9–11] as reviewed in Ref. 12. The more recent findings have reopened the question of the origin of the diffuse sheets in the perovskite ferroelectrics. Recent DXS measurements of cubic $BaTiO_3$ and $KNbO_3$ verified the presence of diffuse sheets,[2] but the underlying mechanism causing the diffuse sheets has remained unresolved. No DXS measurements have been published for cubic $PbTiO_3$. We present here measurements for $PbTiO_3$ because it has similar soft-mode behavior as the other two perovskites in the cubic phase (Fig. 1), yet it has a different local displacement. Cubic $BaTiO_3$ and $KNbO_3$ have disordered local displacements along the $\langle 111 \rangle$ directions, while $PbTiO_3$ has disordered local displacements along the $\langle 001 \rangle$ directions. Thus, one might expect similar diffuse sheets in $PbTiO_3$ if the soft mode was the cause, but possibly different diffuse scattering if the disordered displacements were the cause. We find no DXS sheets in $PbTiO_3$. This result and quantitative calculations give definitive evidence that the soft mode has a negligible contribution to DXS sheets, leading to the conclusion that they are caused by the Comes mechanism. We suggest an explanation for why the $\langle 001 \rangle$ displacements in $PbTiO_3$ do not produce DXS sheets.

The high-quality $PbTiO_3$ single crystals used in this study were grown from stoichiometric melts as has been described elsewhere.[16] DXS measurements were also made on a single crystal of the nonferroelectric perovskite $SrTiO_3$ (Marketech International) at similar elevated temperatures, as an experimental control of thermal *phonon* diffuse scattering (TDS) calculations. All DXS measurements were made at the Pacific Northwest Consortium Collaborative Access Team (PNC-CAT) bending magnet beamline[17] at the Advanced Photon Source (APS). The DXS measurements presented here were all made with the incident photon energy fixed at

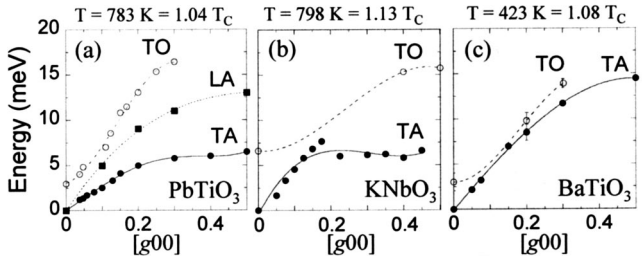

FIG. 1. Phonon dispersion of the lowest energy phonon modes along $[g00]$ measured by inelastic neutron scattering in the cubic phases of (a) $PbTiO_3$ (Ref. 13), (b) $KNbO_3$ (Ref. 14), and (c) $BaTiO_3$ (Ref. 15). The lines are merely guides to the eye.

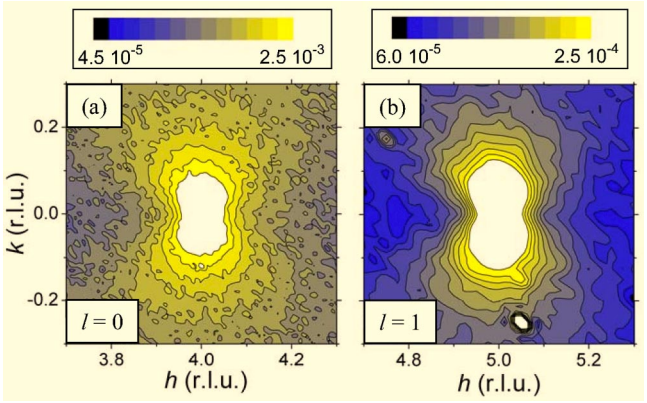

FIG. 2. (Color online) Diffuse scattering profiles from cubic $PbTiO_3$ (T=800 K=1.05 T_C) around the (400) and (501) reflections plotted on a logarithmic scale. (a) The (h, k) plane at l=0. (b) The (h, k) plane at l=1. The "hot spot" at (5.05, −0.25, 1) is due to a weak resolution-limited peak, presumably caused by a multiple-diffraction effect. Note that no diffuse sheet is present along h=5.

12 keV. Sample temperatures as high as 850 K were reached in a vacuum furnace with temperature control within a few degrees. All measurements presented here were made at a fixed sample temperature of 800 K ($\sim$1.05 T_C). The temperature dependence of the diffuse scattering is presented elsewhere.[18]

Figure 2 [where reciprocal space (hkl) are in the (xyz) directions] shows some of the DXS profiles measured around the (400) and (501) reflections in the cubic paraelectric phase of $PbTiO_3$. The Comes and Huller scatterings have the distinctive feature[1,4] of no diffuse scattering on planes that pass through the origin of reciprocal space. Since the k=0 plane in Fig. 2(a) passes through the origin while the l=1 plane in Fig. 2(b) does not, only the l=1 plane can show any Huller and/or Comes scattering. The scattering seen for the k=0 plane can only come from TDS by phonons, while the l=1 plane does not show any sheet scattering that would have as its most distinctive feature intense scattering along the h=5 line. Instead, our analysis shows that the scattering features in both planes are dominated by single phonon (first-order) TDS. The dumbbell-shaped scattering has anisotropy consistent with the directional dependence of the transverse acoustic (TA) and longitudinal acoustic (LA) phonon mode contributions to the scattering, as explained below. Detailed measurements were made throughout the entire Brillouin zones of the (400), (401), and (501) reflections, and no superlattice peaks or diffuse sheets were observed.

The first-order TDS by phonons of wave vector g is described in the high-temperature limit by the equation[19]

$$I_1(\vec{q}) = |F_{hkl}|^2 \frac{Nk_BT}{m} |\vec{q}|^2 \sum_j \frac{\cos^2\alpha_{ij}}{\omega_{ij}^2},$$

where the summation is over the three different jth modes of the ith acoustical or optical phonon. F_{hkl} is the structure amplitude which includes the Debye-Waller factors, k_B is Boltzmann's constant, T is the temperature, m is the mass of the unit cell, $\boldsymbol{q}=\boldsymbol{G}_{hkl}+\boldsymbol{g}$ is the photon transfer wave vector, $\boldsymbol{G}_{hkl}$ is the closest reciprocal lattice vector to $\boldsymbol{q}$, ω_{ij} is the phonon frequency, α is the angle between the phonon displacements and the photon wave vector, and N is a normalization parameter, the only parameter used to fit the experimental data. It should be emphasized that the same value of N is used to fit all the data within a Brillouin zone around a given reciprocal lattice point. In the continuum approximation $\omega=g\nu$, where g is the phonon wave number and ν is its constant velocity. It turns out that the two-phonon scattering processes are not negligible for the case of high-temperature $PbTiO_3$, and can be as high as 10% of the total scattering signal. The second-order TDS, containing no sharp features, has been evaluated using the approximations of Wooster[20] and the methods of Borie.[21] All calculations also included the small contribution from Compton scattering. Before comparing with the theory, all data were corrected for self-absorption. Note that there are no x-ray polarization corrections for a Kappa diffractometer (used in our measurements).

The equation for first-order TDS explains the dumbbell shape found in the measurements shown in Fig. 2. For the case of scattering radiating from the (400) reflection, the cosine term allows contributions from only longitudinal phonons along the h direction, while along the perpendicular l direction only transverse phonons contribute. Since the squares of the LA and TA mode energies are proportional to the cubic elastic constants C_{11} and C_{44}, respectively, the intensity of the diffuse scattering in the two directions for equivalent distances from the (400) reflection is inversely proportional to the elastic constants. The elastic constants for cubic $PbTiO_3$ can be taken from inelastic neutron-scattering measurements shown in Fig. 1(a),[13] yielding the approximate values C_{11}=234 GPa and C_{44}=62 GPa. Consequently, we expect the TDS intensities along these directions to differ by approximately 4 to 1, with the larger intensity along the k direction. Similar arguments apply to the dumbbell surrounding the (501) reflection except that the LA and TA modes are now slightly mixed along the principal axes radiating from the (501) reflection.

Figure 3 shows the comparison between theory and experiment for a TDS calculation beyond the continuum approximation (utilizing the experimental results for $\omega(g)$ shown in Fig. 1(a) along the l direction at h=4 and k=0, where only transverse phonons contribute. We should emphasize the fact that the TA branch along l in cubic $PbTiO_3$ has much smaller values of ω than does the TO soft-mode branch, even quite close to T_C. Since the contribution to diffuse scattering of phonons is proportional to ω^{-2}, the TA branch will dominate the diffuse scattering over the soft mode in all cases, as is verified by a quantitative calculation that shows the soft-mode contribution is usually significantly less than 10% of that of the TA mode. Note from Fig. 1 that TA modes dominate even in $BaTiO_3$ and $KNbO_3$, though not as much as in $PbTiO_3$. This fact alone suggests that the soft-mode branch is not the main factor for producing the diffuse sheets in $BaTiO_3$ and $KNbO_3$.

The calculations of the measured TDS patterns of Fig. 2 require knowledge of the cubic phase acoustic-phonon spectrum as a function of $\boldsymbol{g}$ throughout a (100) plane in a Brillouin zone, which is not available. However, in the continuum approximation, where ω is a linear function of g,

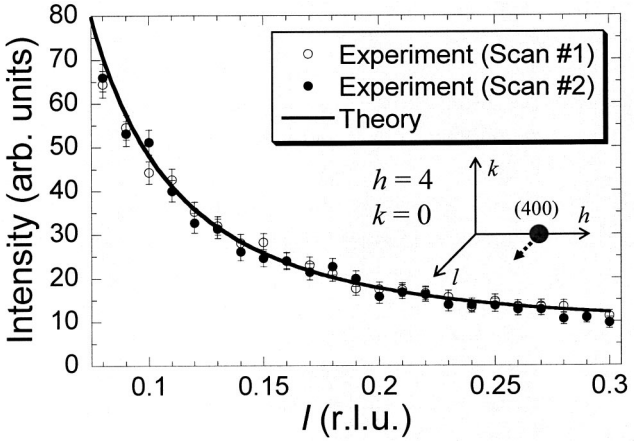

FIG. 3. Comparison between theory and experiment along l at $h=4$ and $k=0$ of cubic $PbTiO_3$, using the measured dispersion of the TA-phonon modes (Ref. 13). Two sets of measurements are presented.

only knowledge of the three elastic moduli of cubic $PbTiO_3$ is required. Figure 1(a) indicates the continuum approximation is valid for $g<0.2$, the region producing the greatest TDS. Figure 4 shows calculations of the experimental TDS profiles presented in Fig. 2 using the continuum approximation. The calculations were made, with the third elastic constant $C_{12}=130$ GPa, chosen so as to best fit the measured diffuse anisotropy in the immediate vicinity of the (400) and (501) reflections, since there have not been any published measurements that we could find at the elevated temperatures of the cubic phase. The TDS theory reproduces all of the features observed in the experimental data. Good agreement between single phonon-scattering theory and experiment was also obtained for $SrTiO_3$, where all of the elastic constants have been measured as a function of the high-temperature range of interest. In the case of $SrTiO_3$ the second-order TDS contribution was calculated to be negligible, and the good agreement was an important check on the accuracy of our calculations and our determination of C_{12} for $PbTiO_3$.

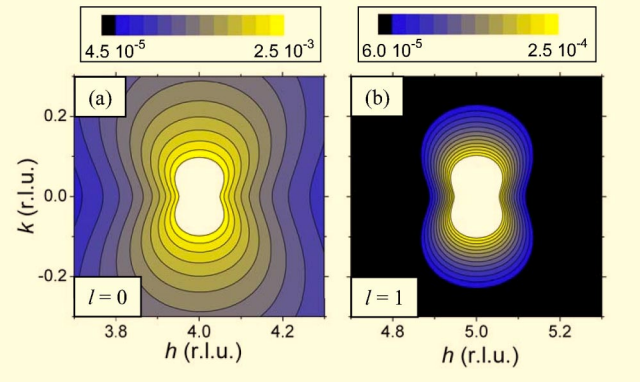

FIG. 4. (Color online) Calculated TDS profiles using the continuum approximation for the measurements presented in Fig. 2. The calculated profiles are quantitatively accurate only within 0.2 r.l.u., beyond which the calculated profiles do not fall off as rapidly as the experimental measurements, due to neglect of phonon dispersion in the calculation.

Diffuse sheets are also found in $KTaO_3$ but another mechanism is required since it is nonferroelectric.[22] XAFS verifies that no disordered local displacements occur in this material. It was suggested that the sheets in $KTaO_3$ occur because the TA-phonon branches in the reciprocal $\langle 100\rangle$ directions have a particularly low $\omega(g)$ that rises rapidly in directions off these axes, giving particularly strong scattering along (100) sheets.[22] This unusual behavior occurs because of a strong interaction between the TA phonon and optical soft-mode branches. Since our measurements and analysis indicate that the DXS sheets found in $BaTiO_3$ and $KNbO_3$ are not produced by the soft-mode model, the question arises whether they occur because of the disordered rhombohedral displacements or by TA phonons as suggested for $KTaO_3$. $BaTiO_3$ and $KNbO_3$ have TA dispersion curves with values above that of $PbTiO_3$ (with $BaTiO_3$ well above and not flattening out at high g), yet our measurements and calculations find no sheets for $PbTiO_3$. In addition, $PbTiO_3$ most closely approximates the $KTaO_3$ TA dispersion curves, but not having its particularly low frequencies. These two observations indicate that the $KTaO_3$ mechanism for sheets is not occurring in these three ferroelectrics. The only remaining mechanism left to explain sheets in $BaTiO_3$ is the Comes model of chains of correlated local displacements. As we argue in the following, a similar mechanism produces sheets in $KNbO_3$.

Although macroscopically the transition at T_C for all three perovskites is similar by changing from tetragonal to paraelectric phases, on a local structure perspective they are quite different. The tetragonal phase for $BaTiO_3$ and $KNbO_3$ has disordered local x and y components not present in the tetragonal phase for $PbTiO_3$. For $BaTiO_3$ and $KNbO_3$ to transform to the cubic phase it is only necessary to disorder the initial z component of the local displacements by reversing this component (by symmetry this does not change the dimensions of the local regions) and then locally disorient the displacements uniformly among the $\langle 111\rangle$ directions (i.e., the eight-site model). Since the transverse components disorder at lower temperatures, the hopping among their sites occurs more rapidly than does the hopping to reverse the displacements among the $\langle 001\rangle$ directions, producing chains of unit cells of local tetragonal regions. The main region where stress is induced by the disordering is where *collinear* chains with reversed tetragonal regions interface. Thus, neighboring parallel, but *noncollinear* chains will have no additional strain energy introduced by either direction of tetragonal regions, producing the cubic phase with Comes chains of unit cells correlated along the $\langle 100\rangle$ directions and no correlation between neighboring chains, leading to the DXS sheets. The chains in $KNbO_3$ are also significant, giving a larger contribution to the sheets by a factor of 1.5 than in $BaTiO_3$, since their DXS is proportional to $(Z\delta)^2$, where Z is the nuclear charge of the atom near the center of the oxygen octahedron and δ is the atom's displacement from the center; δ is 0.17 (0.11) and Z is 22 (41) for Ti (Nb).[7,8]

With the local $\langle 001\rangle$ displacements of $PbTiO_3$ it is not possible to produce the cubic structure by simply reversing the z component because this retains the tetragonal structure. The cubic unit-cell dimension $a_c=(2a+c)/3$, where a is the side of the tetragon base and c is its polar length, requires a

disordering of the *orientation* of the local displacements such that along any cubic axis there are twice the number of tetragonal cells perpendicular to it than along it. The elastic strain induced by a chain of n-oriented tetragonal unit cells in the cubic structure is $n(2/3)(c-a)$, and the elastic energy is minimized by keeping the lengths of chains to a minimum since it increases with n^2. Thus, it is reasonable that the disorder in the $\langle 001 \rangle$ displacements of $PbTiO_3$ is not in finite chains and does not produce sheets of diffuse scattering, but rather produces a broad, featureless background.

Theoretical support of the Comes model came from a theory that predicted the existence of persistent local displacements.[23] Finally, the order-disorder nature of the ferroelectric transition has been reconciled to the large Curie-Weiss factor by a theory that explains the phase transition in terms of an interaction of the local displacements with the soft mode and also naturally explains the central peak.[24]

In conclusion, we have presented DXS measurements from the perovskite ferroelectric $PbTiO_3$ in the high-temperature cubic phase, and find that it has no sheets as occurs in the perovskite ferroelectrics $BaTiO_3$ and $KNbO_3$. A modeling of the DXS with only thermal phonons (including soft modes) reveals that no sheets are produced by this mechanism. The different diffuse scattering in the perovskites can be explained by the different local displacements that persist in the cubic phases. The local $\langle 111 \rangle$ displacements in $BaTiO_3$ and $KNbO_3$ disorder in the cubic phase into correlated finite chains along the $\langle 100 \rangle$ directions and are uncorrelated to their neighboring chains, producing DXS sheets in the $\{100\}$ planes. However, the local $\langle 001 \rangle$ displacements in $PbTiO_3$ do not form local correlated chains because they have only short-range correlations as required to minimize the elastic strain energy introduced by their reorientation in the cubic structure, giving a broad and featureless DXS. Consequently, the DXS features of cubic $PbTiO_3$ are dominated by the acoustic-phonon branches.

The authors thank Y. Yacoby for fruitful discussions and the beamline staff at PNC-CAT for invaluable assistance. Research was supported by DOE Grant No. DE-FGE03-97ER45628. PNC-CAT was supported by DOE Grant No. DE-FG03-97ER45628, the University of Washington, Pacific Northwest National Laboratory, and the Natural Sciences and Engineering Research Council of Canada. Use of the APS was supported by the U.S. DOE-BES under Contract No. W-31-109-Eng-38.

*Present address: National Synchrotron Light Source, Brookhaven National Laboratory, Upton, NY 11973-5000, USA.

†Author to whom correspondence should be addressed; Electronic address: stern@phys.washington.edu

‡Present address: Chonbuk National University, Jeonju, 561-756, South Korea.

[1] R. Comes, M. Lambert, and A. Guinier, Solid State Commun. **6**, 715 (1968); Acta Crystallogr., Sect. A: Cryst. Phys., Diffr., Theor. Gen. Crystallogr. **A26**, 244 (1970).

[2] M. Holma, N. Takesue, and H. Chen, Ferroelectrics **164**, 237 (1995); N. Takesue, M. Maglione, and H. Chen, Phys. Rev. B **51**, 6696 (1995).

[3] W. Cochran, Phys. Rev. Lett. **3**, 412 (1959); W. Cochran, Adv. Phys. **9**, 387 (1960).

[4] A. Huller, Solid State Commun. **7**, 589 (1969); A. Huller, Z. Phys. **220**, 145 (1969).

[5] A. S. Chaves, F. C. S. Barreto, R. A. Norgueira, and B. Zeks, Phys. Rev. B **13**, 207 (1976).

[6] N. Sicron, B. Ravel, Y. Yacoby, E. A. Stern, F. Dogan, and J. J. Rehr, Phys. Rev. B **50**, 13 168 (1994).

[7] B. Ravel, E. A. Stern, R. I. Vedrinskii, and V. Kraizman, Ferroelectrics **206–207**, 407 (1998).

[8] M. I. Bell, K. H. Kim, and W. T. Elam, Ferroelectrics **120**, 103 (1991); V. A. Shuvaeva, K. Yanagi, K. Yagi, K. Sakaue, and H. Terauchi, Solid State Commun. **106**, 335 (1998).

[9] M. D. Fontana, K. Wojcik, H. Idrissi, and G. E. Kugel, Ferroelectrics **107**, 91 (1990).

[10] R. J. Nelmes, R. O. Piltz, W. F. Kuhs, Z. Tun, and R. Restori, Ferroelectrics **108**, 165 (1990).

[11] J.-M. Kiat, G. Baldinozzi, M. Dunlop, C. Malibert, B. Dkhil, C. Menoret, O. Masson, and M.-T. Fernandez-Diaz, J. Phys.: Condens. Matter **12**, 8411 (2000).

[12] Y. Yacoby and E. A. Stern, Comments Condens. Matter Phys. **18**, 1 (1996); E. A. Stern and Y. Yacoby, J. Phys. Chem. Solids **57**, 1449 (1996).

[13] G. Shirane, J. D. Axe, J. Harada, and J. P. Remeika, Phys. Rev. B **2**, 155 (1970).

[14] M. Holma and H. Chen, J. Phys. Chem. Solids **57**, 1465 (1996).

[15] J. Harada, J. D. Axe, and G. Shirane, Phys. Rev. B **4**, 155 (1971).

[16] V. Gavrilyatchenko, A. Semenchev, and E. Fesenko, Ferroelectrics **158**, 31 (1994).

[17] S. M. Heald, D. L. Brewe, E. A. Stern, K. H. Kim, F. C. Brown, D. T. Jiang, E. D. Crozier, and R. A. Gordon, J. Synchrotron Radiat. **6**, 347 (1999).

[18] B. D. Chapman, Ph.D. Dissertation, University of Washington, Seattle, WA, 2003.

[19] B. E. Warren, *X-ray Diffraction* (Dover, New York, 1969).

[20] G. N. Ramachandran and W. A. Wooster, Acta Crystallogr. **4**, 335 (1951).

[21] B. Borie, Acta Crystallogr. **14**, 566 (1961).

[22] R. Comes and G. Shirane, Phys. Rev. B **5**, 1886 (1972).

[23] I. B. Bersuker, Ferroelectrics **164**, 75 (1995).

[24] Y. Girshberg and Y. Yacoby, J. Phys.: Condens. Matter **11**, 9807 (1999).